Nonlinear analysis of the RC structure by higher-order element with the refined plastic hinge

C.K. IU[*]

School of Civil Engineering and Built Environment,Queensland University of Technology, Brisbane, QLD, Australia

Abstract. This paper describes a method of the refined plastic hinge approach in the framework of the higher-order element formulation that can efficaciously evaluate the limit state capacity of a whole reinforced concrete structural system using least number of element(s), whereas the traditional design of a reinforced concrete structure (i.e. AS3600; Eurocode 2) is member-based approach. Hence, in regard to the material nonlinearities, the efficient and economical cross-section analysis is provided to evaluate the element section capacity of non-uniform and arbitrary concrete section subjected to the interaction effects, which is helpful to formulate the refined plastic hinge method. In regard to the geometric nonlinearities, this paper relies on the higher-order element formulation with element load effect. Eventually, the load redistribution can be considered and make full use of the strength reserved owing to the redundancy of an indeterminate structure. And it is particularly true for the performance-based design of a structure under the extreme loads, while the uncertainty of the extreme load is great that the true behaviour of a whole structural system is important for the economical design approach, which is great superiority over the conservative optimal strength of an individual and isolated member based on traditional design (i.e. AS3600; Eurocode 2).

Keywords: refined plastic hinge method; second-order inelastic analysis; one element per member; higher-order element formulation; concrete structures; element load method.

1. Introduction

Concrete material is non-homogenous material, which behaves differently in different load directions that makes concrete material is more difficult to predict than the metal or alloy, since the inelastic deformations of concrete material are due to micro-cracking and internal friction sliding. Also it greatly depends on the material composition that is highly uncertain, which makes the very precise numerical modelling of local concrete behaviour may be meaningless for the engineering applications. For example, a number of researchers (i.e. Cope and Rao (1977); Bergan and Holand (1979); Ma and May (1986)) exploited the plane stress elements for the comprehensive modelling of a concrete member, whose accuracy largely depends on how to model concrete, steel and their mutual interaction and which method of the element discretization being used.

---

*Corresponding author, Ph.D., E-mail: iu.jerryu@gmail.com

To facilitate the design of a concrete structure, the inelastic analysis of the reinforced concrete structure using the beam-column finite element has drawn a great deal of research interests (i.e. Izzuddin *et al.* (1994); Bratina *et al.* (2004)) in the last decades, who based on the plastic zone method, which is desirable to investigate the material effect on the non-uniform reinforced concrete section. Unfortunately, their well-known setback is not efficacious, because the comprehensive stress-strain relationship is needed to characterise the material condition of the element section and the high number of numerical operations are required by stress integration in stress-strain relationship with an allowable error level.

The alternative inelastic analysis is the plastic hinge approach, of which the lump-sum spring stiffness at element ends in terms of the load-deformation relationship characterises the material conditions of the whole element section, this process of which is equivalent to the stress numerical integration. The plastic hinge approach always ensures the reliable numerical convergence thanks to the compatible load-deformation relationship. In addition, it can circumvent the tedious and inefficient stress integration technique.

The cross-section analysis is the technique of element loading state evaluation, particularly helpful to the non-uniform and arbitrary element section. In the framework of the plastic zone approach, a few scholars (i.e. Izzuddin and Lloyd Smith (2000); Chiorean (2004)) presented the cross-section analysis to build the axial and bending interaction capacity curve of the element section. Based on the plastic hinge approach, Liu *et al.* (2012a) developed the cross-section analysis for the element section from the previous research work by Chen *et al.* (2001). Iu (2008) developed the cross-section analysis for the non-uniform and arbitrary composite beam sections without bending and axial interaction effect. As a result, the design interaction equation is needed.

The new system design approach of the RC structure using least number of element(s) is to account for the true performance of a whole structure, when the modelling capacity of the method is competent, which exploits the refined plastic hinge method in the context of the higher-order finite element formulation with element load effects.

2. Higher-order displacement-based element with element load effect

The deformations comprise the deformations u in the x direction, v in the y direction, w in the z direction and the twist ϕ about the x-axis. Based on the co-rotational coordinate system, the dependent variables of transverse deflections v and w are replaced by nodal rotations as θ_z and θ_y, about z- and y-axis, respectively, such as $\mathbf{u} = \{u, \theta_y, \theta_z, \phi\}^{\mathrm{T}}$. These rotations are the dependent variables in turn which define the transverse deflections in the element stiffness formulation.

The higher-order transverse displacement interpolation function of an element given in Eq. (1) not only fulfils the essential boundary condition (compatibility condition) in Eqs. (2) - (3), but also natural boundary condition (force equilibrium equation) in Eqs. (4) - (5), as originally proposed by Chan and Zhou (1994). The equivalent mid-span moment M_0 and shear force S_0 are respectively introduced into Eqs. (7)-(8), which enable to measure additional deflection and loading distribution due to element load effect (Iu and Bradford (2015); Iu (2015)).

$$v(x) = \sum_i^p c_i x^i \tag{1}$$

in which c_i is unknown coefficient solved from boundary conditions given from Eqs. (2) to (8); p

is polynomial of order up to 5 in this sense. In the transverse deflection v in the y direction,

$$v = 0 \quad \text{and} \quad \frac{\partial v}{\partial x} = \theta_{z1} \quad \text{at } \zeta = 0 \tag{2}$$

$$v = 0 \quad \text{and} \quad \frac{\partial v}{\partial x} = \theta_{z2} \quad \text{at } \zeta = 1, \tag{3}$$

while the equilibrium equation of bending and shear force given by

$$EI_z \frac{\partial^2 v}{\partial x^2} = Pv - M_{z1}(1-\zeta) + M_{z2}\zeta + M_0 \tag{4}$$

$$EI_z \frac{\partial^3 v}{\partial x^3} = P\frac{\partial v}{\partial x} + \frac{M_{z1} + M_{z2}}{L} + S_0 \tag{5}$$

$$\text{where } \zeta = \frac{x}{L}. \tag{6}$$

$$EI_z \frac{\partial^2 v}{\partial x^2} = Pv + \frac{M_{z2} - M_{z1}}{2} + M_0 \quad \text{at } \zeta = \tfrac{1}{2} \tag{7}$$

$$EI_z \frac{\partial^3 v}{\partial x^3} = P\frac{\partial v}{\partial x} + \frac{M_{z1} + M_{z2}}{L} + S_0 \quad \text{at } \zeta = \tfrac{1}{2} \tag{8}$$

and leads to the deformation

$$
\begin{aligned}
v = & \left\{ \left[\zeta - \frac{\frac{1}{2}(48+5q)}{48+q}\zeta^2 + \frac{4q}{48+q}\zeta^3 - \frac{2q}{48+q}\zeta^4 \right] \right. \\
& + \left. \left[-\frac{\frac{1}{2}(240+7q)}{80+q}\zeta^2 + \frac{80+9q}{80+q}\zeta^3 - \frac{10q}{80+q}\zeta^4 + \frac{4q}{80+q}\zeta^5 \right] \right\} L\theta_{z1} \\
& + \left\{ \left[\frac{\frac{1}{2}(48+5q)}{48+q}\zeta^2 - \frac{4q}{48+q}\zeta^3 + \frac{2q}{48+q}\zeta^4 \right] \right. \\
& + \left. \left[-\frac{\frac{1}{2}(240+7q)}{80+q}\zeta^2 + \frac{80+9q}{80+q}\zeta^3 - \frac{10q}{80+q}\zeta^4 + \frac{4q}{80+q}\zeta^5 \right] \right\} L\theta_{z2} \\
& - \frac{\overline{M}_0 L}{48+q}\left[\zeta^2 - 2\zeta^3 + \zeta^4\right] + \frac{\overline{S}_0 L^2}{80+q}\left[\zeta^2 - 4\zeta^3 + 5\zeta^4 - 2\zeta^5\right]
\end{aligned}
\tag{9}
$$

$$\text{or } v = N_1 L\theta_{z1} + N_2 L\theta_{z2} - N_m L\overline{M}_0 + N_s L^2 \overline{S}_0 \tag{10}$$

$$\text{in which } q = \frac{PL^2}{EI}. \tag{11}$$

The transverse deflection w in the z direction is in a similar fashion. N_1, N_2, N_m and N_s are displacement functions with respect to rotations at first and second node, and element load contributed from moment and shear force components, respectively; the equivalent mid-span moment $\overline{M}_0$ and shear force $\overline{S}_0$ are given under the different sorts of element load, which accounts for the element load effect at the element level and comprehensively discussed in Iu and Bradford (2015) and Iu (2015); q is axial load parameter.

3. Stiffness formulation for higher-order element with element load effects

The derivation of the stiffness formulation of the higher-order element with element load effects can be by virtue of the virtual work principle. Finally, the secant stiffness formulation or element resistance formulation can be obtained as,

$$
\begin{aligned}
M_{\alpha 1} = \frac{\partial U}{\partial \theta_{\alpha 1}} = \frac{EI_\alpha}{L} & \left[\frac{19200 + 800q + \frac{61}{7}q^2 + \frac{23}{1260}q^3}{(80+q)^2} + \frac{2304 + 288q + \frac{29}{5}q^2 + \frac{11}{420}q^3}{(48+q)^2} \right] \theta_{\alpha 1} \\
+ \frac{EI_\alpha}{L} & \left[\frac{19200 + 800q + \frac{61}{7}q^2 + \frac{23}{1260}q^3}{(80+q)^2} - \frac{2304 + 288q + \frac{29}{5}q^2 + \frac{11}{420}q^3}{(48+q)^2} \right] \theta_{\alpha 2} \quad (12) \\
+ \frac{EI_\alpha}{L} & \left[-\frac{q^2\overline{M}_0}{210(48+q)^2} - \frac{q^2\overline{S}_0 L}{630(80+q)^2} \right]
\end{aligned}
$$

$$\text{or } M_{\alpha 1} = \frac{EI_\alpha}{L}\left(C_1 \theta_{\alpha 1} + C_2 \theta_{\alpha 2} - C_m \overline{M}_0 - C_s \overline{S}_0 L \right), \tag{13}$$

$$
\begin{aligned}
M_{\alpha 2} = \frac{\partial U}{\partial \theta_{\alpha 2}} = \frac{EI_\alpha}{L} & \left[\frac{19200 + 800q + \frac{61}{7}q^2 + \frac{23}{1260}q^3}{(80+q)^2} + \frac{2304 + 288q + \frac{29}{5}q^2 + \frac{11}{420}q^3}{(48+q)^2} \right] \theta_{\alpha 2} \\
+ \frac{EI_\alpha}{L} & \left[\frac{19200 + 800q + \frac{61}{7}q^2 + \frac{23}{1260}q^3}{(80+q)^2} - \frac{2304 + 288q + \frac{29}{5}q^2 + \frac{11}{420}q^3}{(48+q)^2} \right] \theta_{\alpha 1} \quad (14) \\
+ \frac{EI_\alpha}{L} & \left[\frac{q^2\overline{M}_0}{210(48+q)^2} - \frac{q^2\overline{S}_0 L}{630(80+q)^2} \right]
\end{aligned}
$$

$$\text{or } M_{\alpha 2} = \frac{EI_\alpha}{L}\left(C_1 \theta_{\alpha 2} + C_2 \theta_{\alpha 1} + C_m \overline{M}_0 - C_s \overline{S}_0 L \right) \tag{15}$$

in which the subscript α denotes y or z, and

$$P = P_1 - P_2 = \frac{\partial U}{\partial e} + \frac{\partial U}{\partial q} \cdot \frac{\partial q}{\partial e}$$

$$= \frac{EAe}{L} + EA \sum_{\alpha=y,z} \left[b_1 \left(\theta_{\alpha 1} + \theta_{\alpha 2} \right)^2 + b_2 \left(\theta_{\alpha 1} - \theta_{\alpha 2} \right)^2 \right.$$

$$\left. + b_{m1} \left(\theta_{\alpha 1} - \theta_{\alpha 2} \right) \overline{M}_0 + b_{s1} \left(\theta_{\alpha 1} + \theta_{\alpha 2} \right) \overline{S}_0 L + b_{m2} \overline{M}_0^2 + b_{s2} \overline{S}_0^2 L^2 \right] \qquad (16)$$

$$= EA \left[\frac{e}{L} + \sum_{\alpha=y,z} \left(C_b + b_{m1} \left(\theta_{\alpha 1} - \theta_{\alpha 2} \right) \overline{M}_0 + b_{s1} \left(\theta_{\alpha 1} + \theta_{\alpha 2} \right) \overline{S}_0 L + b_{m2} \overline{M}_0^2 + b_{s2} \overline{S}_0^2 L^2 \right) \right]$$

in which

$$b_1 = \frac{12800 + 2080q/7 + 46q^2/21 + 23q^3/2520}{\left(80 + q \right)^3} \qquad (17)$$

$$b_2 = \frac{4608 + 672q/5 + 66q^2/35 + 11q^3/840}{\left(48 + q \right)^3} \qquad (18)$$

$$b_{m1} = \frac{-16q}{35 \left(48 + q \right)^3} \qquad (19)$$

$$b_{m2} = \frac{12/35 + q/105}{\left(48 + q \right)^3} \qquad (20)$$

$$b_{s1} = \frac{-16q}{63 \left(80 + q \right)^3} \qquad (21)$$

$$b_{s2} = \frac{20/63 + q/315}{\left(80 + q \right)^3} \qquad (22)$$

Right subscript symbol m and s in Eqs. (17) - (22) stand for the contribution from moment and shear force component, respectively. C_m and C_s provoke the second-order moment from the moment $\overline{M}_0$ and shear force $\overline{S}_0$ components respectively due to coupling effect of both axial loads and lateral element loads, whereas b_{m1}, b_{m2}, b_{s1} and b_{s2} exhibit axial force resistance subjected to the coupling effect between the axial loads and the lateral element loads.

4. Cross-section analysis of non-uniform and arbitrary RC section

According to the plastic hinge approach, the yield function of the element section is required to
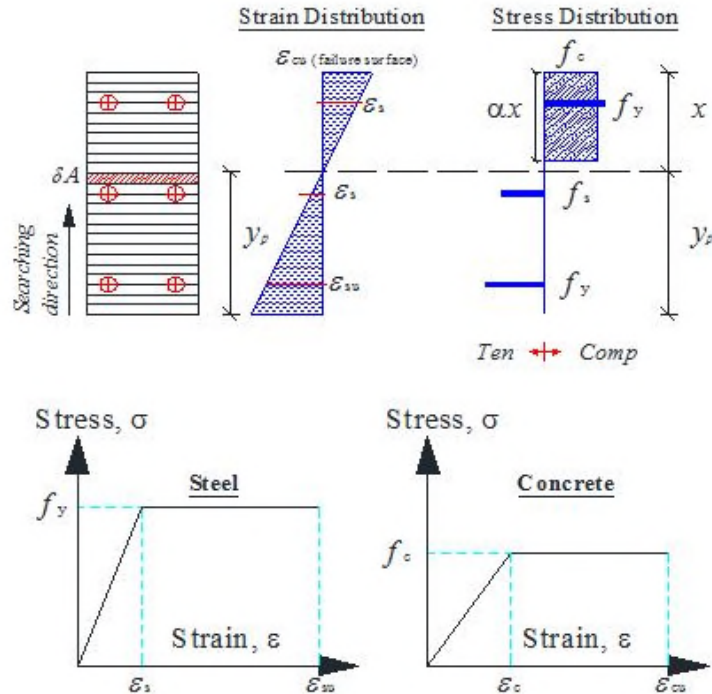
Fig. 1 Material laws and stress-strain distribution of reinforced concrete section

identify its material condition in the load-deformation relationship. Therefore, a cross-section analysis is necessarily proposed in this study in the simple and efficient manner in order to regulate the material condition across the non-uniform and arbitrary element section under interaction effect by using a unique set of yield functions.

To extend from Iu (2008) to any axial load level in the interaction curve, the algorithm of the proposed cross-section analysis is to scrutinise the layer δA as the depth of neutral axis y_p, at which the condition of $\int \sigma dA = P_c$ at the specific axial load level P_c is satisfied. When the depth of neutral axis y_p is assumed, the failure surface is thus determined in Fig. 1. Eventually, the failure strain distribution profile is obtained and written as Eq. (23),

$$\varepsilon = \phi(y - y_c) \tag{23}$$

which is also known as the failure compatibility condition. The curvature ϕ is obtained from the failure surface ε_{cu} and depth of neutral axis y_p. It is interesting to note that since the ductility of the concrete material far less compared to those of the steel material (i.e. ε_{cu} (0.003) $<< \varepsilon_{su}$ (0.02)), the failure surface of the reinforced concrete section is always dictated by the compression in concrete, except for the very high-strength steel reinforcement whose ductility is very low.

The material law of the concrete and steel reinforcement are simplified as the bi-linear relation for the practical design aim as shown in Fig. 1, but not limited to, when the algorithm of the proposed cross-section analysis can expand to the multi-linear stress-strain relation for comprehensive material study, such as strain-hardening region. However, more parameters are
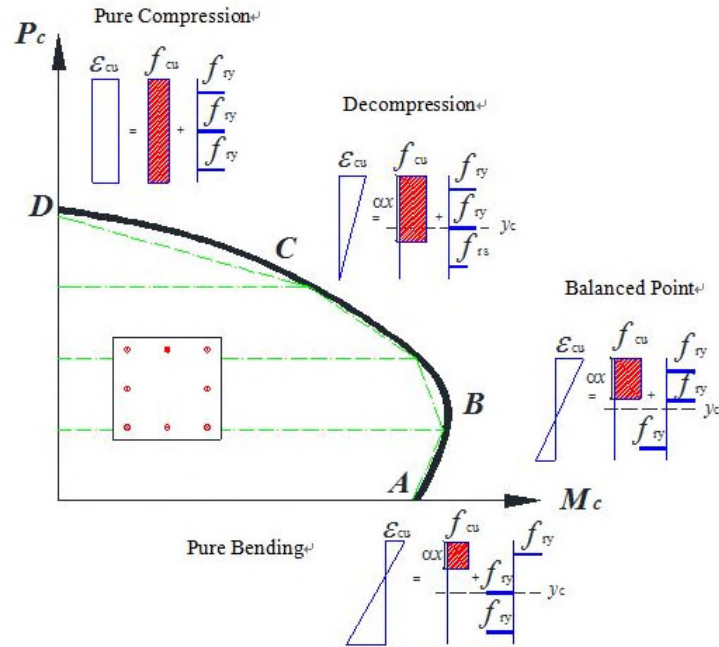
Fig. 2 Interaction profile of the reinforced concrete section with special loading state

required for multi-linear relation and thus hinder the application of design.

While the strain ε_s of the steel reinforcement exceeds yield strain ε_y according to the linear compatibility condition of Eq. (23), the yield stress f_y is attained at that steel reinforcement. Otherwise, the elastic stress of steel reinforcement complies with the elasticity Hooke law, such as $f_s=E_s\varepsilon$. However, the concrete fibre does not always follow the compatibility condition strictly, whose capacity is derived as the ideal compressive stress f_c times a portion α of the depth of plastic neutral axis y_p for the simplified ideal compressive stress block as illustrated in Fig. 1. The factor of α is normally taken as 0.8 in this study.

Therefore, once the failure compatibility condition according to a particular y_p is computed, at which the axial force equilibrium,

$$P_c = \int \sigma dA \tag{24}$$

is sought at specific axial load level P_c or its difference is less than the axial load of a strip of layer (i.e. $\delta P_c \le \sigma \delta A$). In the meantime, the overall moment capacity M_c of the section can be given by,

$$M_c = \int \sigma(y - y_c) dA \tag{25}$$

This procedure is further repeated for other axial load level P_c until the whole interaction capacity curve of the element section completes as illustrated in Fig. 2. However, this procedure is valid if and only if the neutral axis (i.e. y_c or y_p) lies within the element section. It heralds that the above procedure is only applicable between the decompression and pure bending as shown in Fig.2. Because of this, the interaction capacity curve between decompression and pure axial
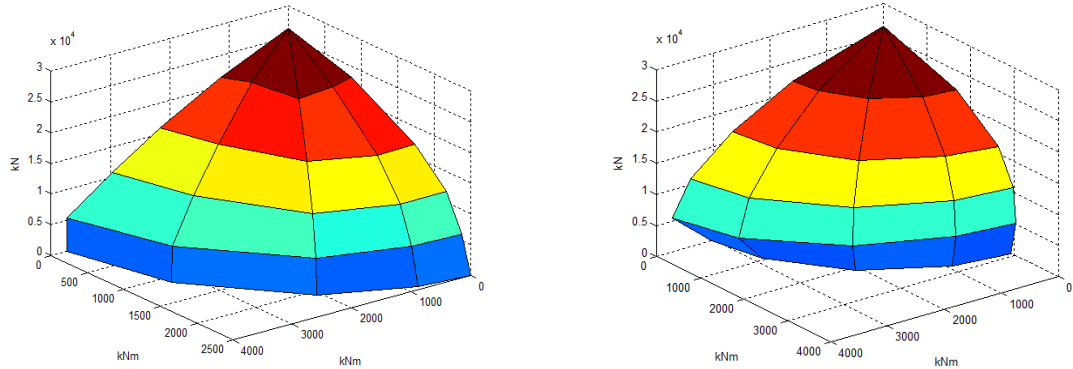
(a) Section with high steel to concrete ratio   (b) Section with low steel to concrete ratio

Fig. 3 Three-Dimensional interaction profile of concrete section

compression as well as between pure bending and axial tension is assumed linear without loss of accuracy. The number of specific axial load level P_c between the decompression and pure bending can define the fineness of the interaction capacity curve. In this proposed cross-section analysis, 3 specific axial load levels are required to construct the capacity curve between decompression and pure bending piecewise, which is derived by a fraction (i.e. ¼; ½; ¾) of the axial capacity at decompression P_c as indicated in Fig. 2. Hence, there are total 7 ordinates (i.e. M_c & P_c) to define the interaction capacity curve of a particular non-uniform and arbitrary reinforced concrete section by a set of the linear equations as depicted by the dash lines in Fig. 2.

For the domain of the biaxial bending, this cross-section analysis relies on the well-developed interaction capacity curve from design codes (i.e. AS3600; Eurocode 2) as written in Eq. (26),

$$\left(\frac{M_x}{M_{cx}}\right)^{\alpha_n} + \left(\frac{M_y}{M_{cy}}\right)^{\alpha_n} \leq 1 \tag{26}$$

in which M_{cx} and M_{cy} are respectively moment capacity about major and minor axis at the particular axial load level P_c, which can be derived from Eq. (25) for the respective axis; α_n is the parameter to control the shape of biaxial interaction capacity curve, whose value is $1 \leq \alpha_n \leq 2$. When α_n is equal to 1, it means linear biaxial bending relation, which is very conservative, whereas α_n is 2 for circular biaxial bending relation, which is very economical but sometimes unsafe. Therefore, the three-dimensional (i.e. P_c, M_{cx}, M_{cy}) interaction capacity curve is constructed as illustrated in Fig. 3.

Unlike the other cross-section analysis (i.e. Chiorean (2010); Liu *et al.* (2012a)), they can generate the comprehensive three-dimensional interaction capacity curve but computational demanding. On the other hand, the benign feature of the proposed cross-section analysis is to locate a unique set of discrete critical loading states (i.e. P_c, M_{cx}, M_{cy}), which can define the three-dimensional interaction capacity curve, in advent of the numerical procedures without demanding computational storage, and further this cross-section analysis is no longer implemented in the course of the nonlinear solution procedures and thereby without demanding computational operation.

It is noteworthy that the interaction capacity curve of the reinforced concrete section normally

characterises with the strength enhancement in moment capacity at balanced point B compared to the pure bending state at A as indicated in Fig. 2, because the compression in concrete can contribute to the massive moment capacity enhancement by lowering the plastic neutral axis y_p from those at pure bending state, which implies increase in lever arm and larger compression portion. On contrary, the steel section cannot provide such large moment capacity enhancement owing to the inconsiderable steel section.

5. Flexural stiffness of the concrete element at pre-yield stage

The concrete cracking due to tension can affect the flexural behaviour significantly at the pre-yield regime, which results in larger deflection. The present method therefore adopts the effective second moment of area I_{eff} in Eq. (27) proposed by Branson and Metz (1963), which offers a reasonable estimation of the pre-yield behaviour in the simple and effective manner and thereby is widespread in the analyses for the reinforced concrete structures,

$$ I_{eff} = I_{cr} + \left(I_g - I_{cr} \right) \left(\frac{M_{cr}}{M} \right)^3 \tag{27} $$

whose principle is to model the localised flexural cracking phenomenon by equivalent flexural stiffness of a whole element section, which is bounded by $I_{cr} \leq I_{eff} \leq I_g$; I_g and I_{cr} are respectively second moment of area of gross section and cracked section, which can be obtained from the present cross-section analysis; M_{cr} and M are the cracking moment capacity and bending moment of the member, respectively. In this study, the ratio of (M_{cr}/M) in Eq. (27) is kept constant in the course of the nonlinear solution procedure, because it maintains the high level of efficiency. Therefore, the constant effective second moment of area I_{eff} in between I_{cr} and I_g, is reasonable and accurate in the integral sense. By contrary, the effective second moment of area I_{eff} commensurate to the latest load level is unreliable, because the solution procedure traces the nonlinear equilibrium path of which depends on the loading states. As a result, the approach with updated loading state may provoke the issue of path dependent, as the load increment can determine the load states but it in turn affects the equilibrium path itself. The similar phenomenon reported in Zienkiewicz and Taylor (1991) that the material nonlinear effect can have the path-dependent effect. On the other hand, the plastic hinge approach has not encountered of this problem when assuming the elastic element stiffness formulation, which is irrelevant to the loading state of an element. Therefore, for the robust, efficient and reliable standpoint, the constant effective second moment of area I_{eff} is adopted in this study.

6. Refined plastic hinge method for a concrete element at post-yield stage

Post-yield behaviour is essential to the performance-based design approach, while the true performance of a whole structure is of much concern. Iu and Chan (2004) developed the nonlinear fire analysis of a steel frame, in which the strain-hardening effect in terms of engineering plasticity was first introduced in the plastic hinge approach. Further, Iu *et al*. (2009) presented the refined plastic hinge approach, which includes the inelastic effects under interaction effect. This plastic hinge approach with the present cross-section analysis can therefore capture the inelastic buckling

of a member by itself. The incremental refined plastic hinge stiffness for the beam-column concrete element at post-yield stage is given as,

$$\Delta S = \frac{EI}{L}\left(\frac{1-\phi_f(\mathbf{f})}{\phi_i(\mathbf{f})-1}+\mu\right) \tag{28}$$

in which the incremental spring stiffness ΔS is such that $\infty > \Delta S > 0$; μ is strain-hardening parameters; $\phi_i(\mathbf{f})$ and $\phi_f(\mathbf{f})$ are the initial yield and interaction capacity curve, respectively, in which $\mathbf{f}$ is load vector or element loading state. The interaction capacity curve $\phi_f(\mathbf{f})$ is founded by a unique sets of discrete points with respect to each axis generated from the present cross-section analysis, whereas the initial yield function $\phi_i(\mathbf{f})$ is given as,

$$\phi_i(\mathbf{f}) = \frac{P}{P_c} + \frac{M_x}{M_{cx}} + \frac{M_y}{M_{cy}} \tag{29}$$

in which M_{cx} and M_{cy} are the moment capacity, which can be either plastic moment capacity M_p (i.e. $Z_p \cdot f_c$) or elastic moment capacity M_e (i.e. $Z_e \cdot f_c$); The higher-order element with the refined plastic hinge stiffness formulation are comprehensively discussed in Iu and Bradford (2012). Under a particular circumstance (i.e. the bending dominant element), the incremental spring stiffness in Eq. (28) can be reduced to,

$$\Delta S = \frac{EI}{L}\left(\frac{M_p - M}{M - M_e}+\mu\right) \tag{30}$$

For the bending beam element, Eq. (30) is adopted similar to those used in Iu and Chan (2004) and Liu *et al*. (2012b).
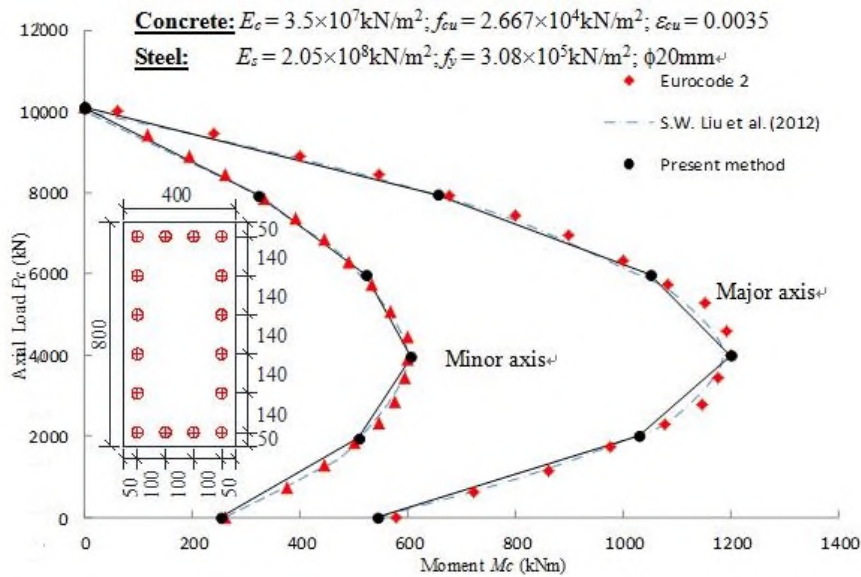

Fig. 4 Ultimate section capacity of rectangular reinforced concrete section
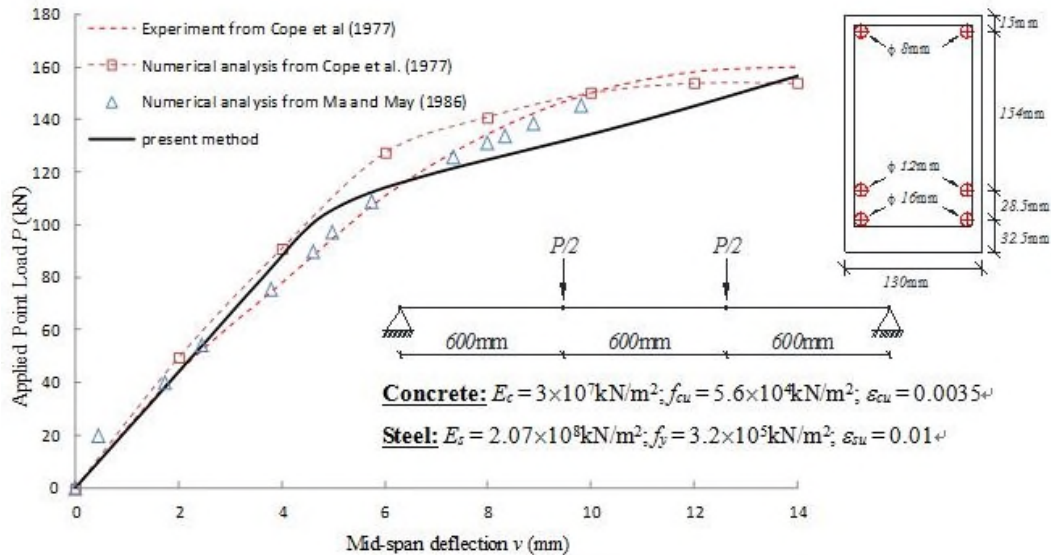
Fig. 5 Mid-span deflections of a simple rectangular RC beam subjected to 2 point loads

7. Numerical examples

In this verification section, a number of examples are examined in this paper, including the section capacity, a few simple reinforced concrete members as well as a concrete frame.

7.1 Ultimate capacity of RC section under interaction between axial load and bending

A rectangular reinforced concrete section under interaction effect was presented by Liu *et al*. (2012a), whose layout of the section and properties are given in Fig. 4. The interaction capacity curves about both major and minor axes from the present cross-section analysis are very consistent with the others, including Eurocode 2 and Liu *et al*. (2012a). It can be seen that, in the major bending direction, the enhancement in moment capacity is greater than those in minor axis, when the large lever arm from the plastic centroid y_p to the concrete compression is accommodated. This kind of phenomenon is easily found in the concrete section with low steel to concrete ratio as illustrated in Fig. 3.

7.2 A simple supported rectangular reinforced concrete beam with strain-hardening effect

A simply supported rectangular reinforced concrete beam is subjected to 2 point loads. The geometry and its section properties are shown in Fig. 5, which was experimentally and numerically investigated by Cope and Rao (1977) and Ma and May (1986) numerically. In their numerical studies, the comprehensive finite element meshes were required for the reinforced concrete beam, which was based on the two-dimensional plane stress elements. The present approach uses 3 one-dimensional higher-order elements for this simply supported beam as given in Fig. 5 in order to capture material effects at load applications.
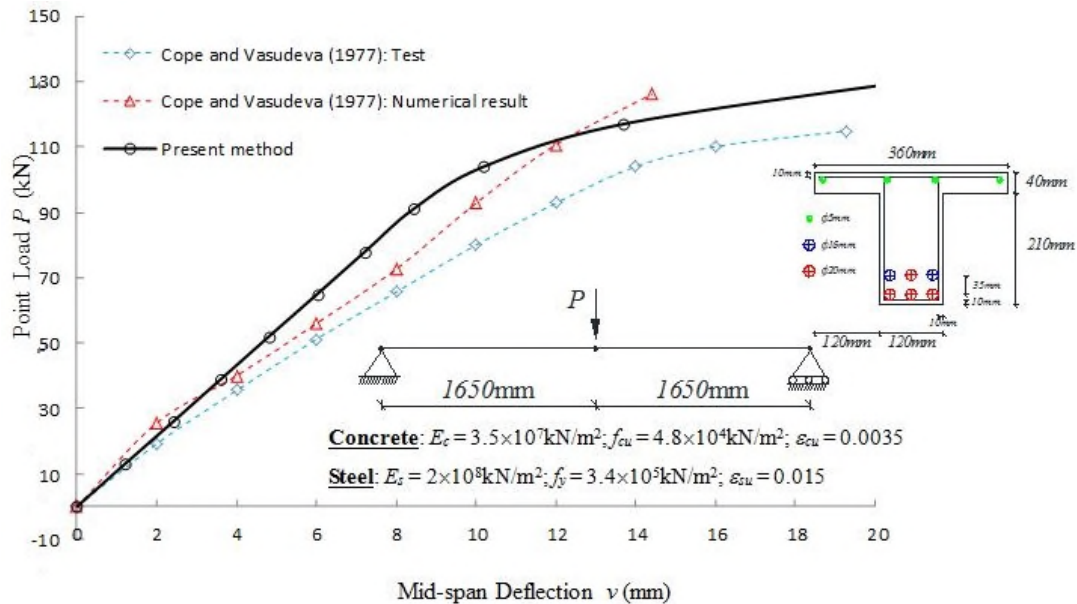
Fig. 6 Mid-span deflection of a simple supported RC T-beam

Fig. 5 indicates the mid-span deflections of the concrete beam against the total point load *P*. In the elastic range, the load-deflection curve from the present method is in between the experimental and numerical approach (Cope and Rao (1977)). And the concrete beam reaches its full plasticity at the level of 120kN from the present method similar to Ma and May (1986). And the post-yield behaviour of this concrete beam from the present method is also consistent with others as shown in Fig. 5. Therefore, the present method can yield the accurate solutions in the efficient manner with least number of elements when compared to Cope and Rao (1977) and Ma and May (1986).

7.3 Ultimate strength of a simple supported reinforced concrete T-beam

This example investigates the behaviour of the T-shape reinforced concrete beam under a point load at mid-span, which was studied by Cope and Rao (1977) experimentally and numerically. In their numerical modelling, the concrete T-beam is simulated by the three-dimensional comprehensive element mesh using the plane stress finite elements. On contrary, the present method divides a simple supported T-beam into 2 higher-order finite elements so as to capture the material yielding by a plastic hinge at mid-span.

Fig. 6 plots the mid-span deflection of the concrete T-beam with the applied point load *P* from Cope and Rao (1977) and the present method. It is observed that the discrepancy of the mid-span deflections between the present method and experimental result becomes apparent while applied load *P* increases, because the severe cracking was measured. In spite of this, the present method can average the nonlinear pre-yield behaviour when compared to the comprehensive numerical modelling. The ultimate load of the concrete T-beam was measured at *P*=127kN (Cope and Rao (1977)), and the present method can predict it at *P*=130kN, which are very consistent. All in all, the present method is accurate in modelling capacity but more efficient and effective when using the least number of elements.
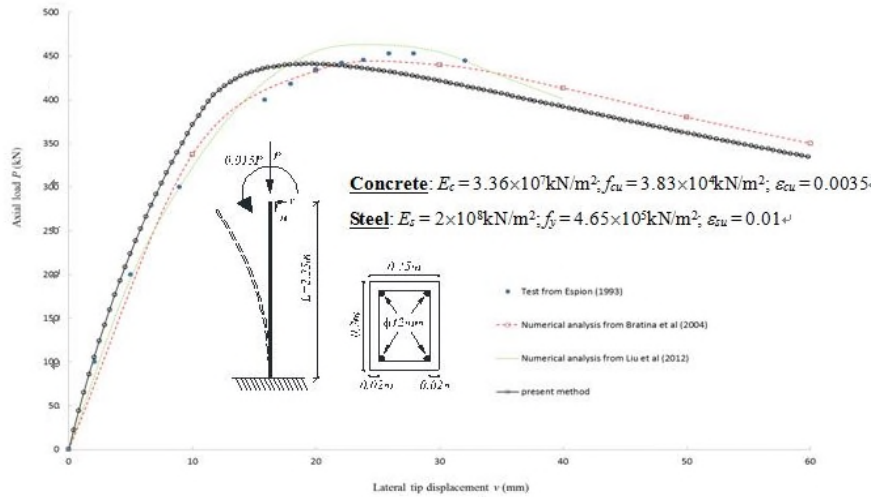
Fig. 7 Lateral tip displacement vs axial compressive load of the Foure's RC column
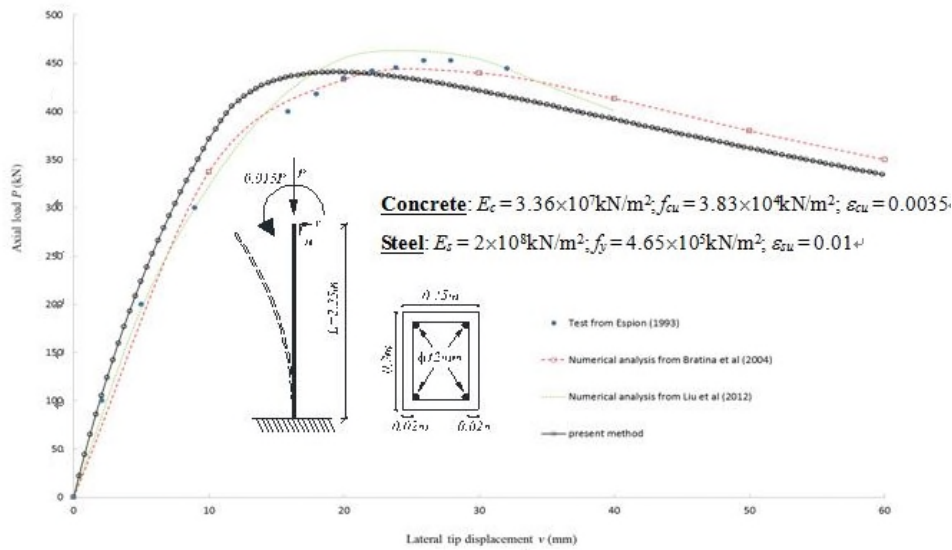
Fig. 8 Interaction capacity curve of the Foure's RC column

7.4 A Cantilever concrete column encountering the stiffness degradation due to P-Δ effect

A cantilever reinforced concrete column (Foure's column) was tested by Espion (1993) as one of the benchmark examples to verify the accuracy of nonlinear analysis of the RC structures. This column is subjected to an axial compression load P and eccentric moment $0.015P$, so it is critical to the P-Δ effect and its interaction between bending and axial compression.

The lateral tip displacement v against the axial compression P is plotted in Fig. 7. In the onset of elastic range, there is an offset after 100kN at which the column begins cracking. Despite this

Table 1 Material and section properties of the concrete frame

Material	Elasticity (kN/m^2)		Yield stress (kN/m^2)		Ultimate strain (%)
Concrete:	3.15×10^7		3.6×10^4		0.035
Steel:	2×10^8		2.93×10^5		0.015
Section	Z_e (m^3)	Z_p (m^3)	I_g (m^4)	I_{cr} (m^4)	Yield surface
1	0.24495×10^{-3}	0.29317×10^{-3}	0.40062×10^{-4}	0.19361×10^{-4}	Eq. (30)
2	0.26836×10^{-3}	0.29421×10^{-3}	0.43694×10^{-4}	0.20395×10^{-4}	Eq. (30)
3	0.24495×10^{-3}	0.28904×10^{-3}	0.40062×10^{-4}	0.19361×10^{-4}	Eq. (30)
4	0.24495×10^{-3}	0.29317×10^{-3}	0.40062×10^{-4}	0.19361×10^{-4}	Eq. (28)
5	0.24495×10^{-3}	0.28904×10^{-3}	0.40062×10^{-4}	0.19361×10^{-4}	Eq. (28)
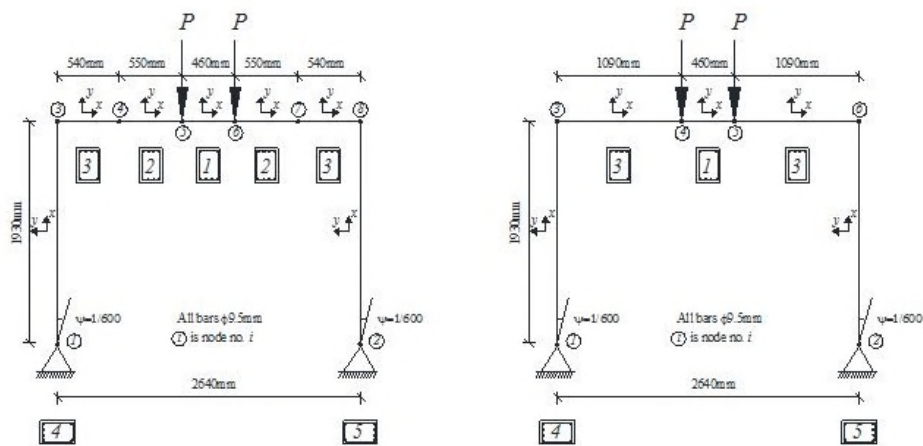
a) Detailed modelling of the frame   b) Simple modelling of the frame (case
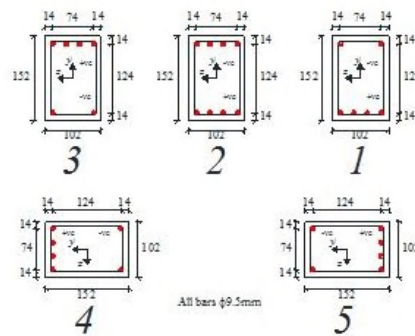
c) Section layouts of the concrete frame

Fig. 9 Numerical modelling details of the simple portal concrete frame

slight discrepancy at the elastic regime, the present method can offer the consistent load-deflection behaviour with the other approaches (i.e. Bratina *et al.* (2004), Liu *et al.* (2012)) as shown in Fig. 7 as well as the accurate ultimate load 441kN when compared to experimental and numerical results
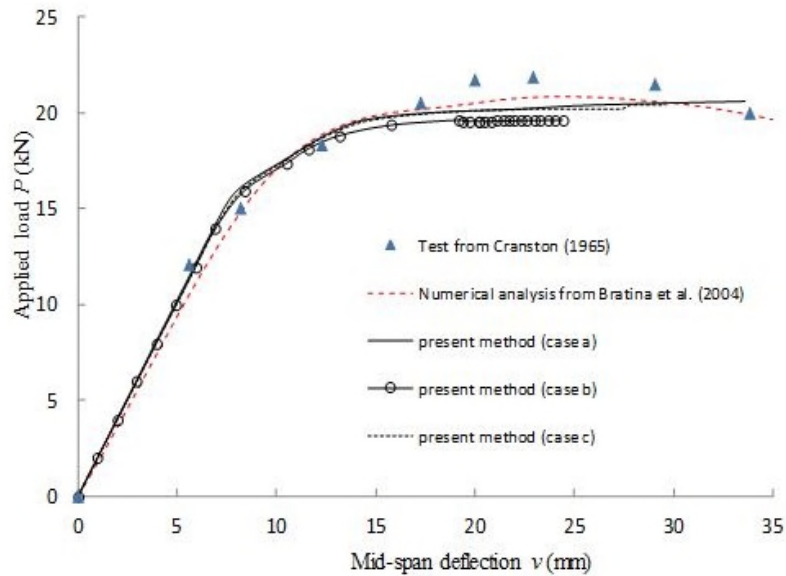
Fig. 10 Mid-span deflection of the concrete beam of the Cranston's frame

454kN (Espion (1993)) and 447kN (Bratina *et al*. (2004)), respectively. After the ultimate load, the present method can predict that the stiffness and strength of the Foure's column deteriorates due to the P-Δ effect, when the lateral displacement increases in Fig. 7 with the loading state decreasing in Fig. 8 till a mechanism at its base.

7.5 A simple portal concrete frame with pinned supported at its column bases

A reinforced concrete portal frame (Cranston's frame) was tested by Cranston (1965) and numerically analysed by a few scholars, including Sun *et al*. (1994), Bratina *et al*. (2004) and Liu *et al*. (2012). The geometry of the Cranston's frame is illustrated in Fig. 9; Figure 9(a) is the original detailed numerical modelling of the Cranston's frame (case a), whereas the Figure 9(b) is the simplified modelling (case b), which investigate the numerical modelling effect for the better behavioural evaluation. The details of the sections are given in Fig. 9(c).

The material and section properties are listed in Table 1. Their second moment of area I_g and I_{cr} of gross and cracked section are same, because I_g disregards the direction of loading distribution and I_{cr} possesses the same detailing arrangement with respect to the loading distribution. On contrary, the plastic modulus Z_p of the sections are a bit different, for example Z_p of the sections 1&4 slightly defers from the sections 2&5 in Fig. 9(c), because the concrete exhibits different capacity in different loading directions at inelastic range. It is reminded that the numerical modelling of the reinforced concrete structure is dependent on the detailing arrangement and loading distribution of the priori behavioural pattern.

The mid-span deflections of the concrete beam against the applied loads *P* are plotted in Fig. 10. The present method with the detailed modelling (case a) can compute the behaviour of the Cranston's frame in the very consistent manner with those from Bratina *et al*. (2004). The ultimate

load from the present method (i.e. *P*=20.4kN) is slightly lower than the tested result (Cranston (1965)) (i.e. *P*=21.1kN). Further, the present method with the simplified modelling (case b) can predict its ultimate load (i.e. *P*=19.6kN) lower than those by using the detailed modelling (case a) as shown in Fig. 10, because the section capacity (i.e. Z_p) of section 3 is only a bit lower than those of section 2 as given in Table 1. If the section 2 in the original modelling (case a) in Fig. 9(a) replaces with the section 1 as regarding another modelling (case c), whose load-deflection behaviour and ultimate load are all well-agreed with those of (case a) as illustrated in Fig. 10, because the region from node 4 to 7 in Fig. 9(a) are most likely under sagging moment, and the section 1 can capture the significant flexural behaviour of the original detailing of the Cranston's frame.

It heralds that the accuracy of the integrated analysis and design of the reinforced concrete structure relies on the numerical modelling in alignment with its priori behavioural pattern, especially when the behaviour of the non-homogenous concrete member section is extreme with respect to the loading distribution.

8. Concluding remarks

In summary, the present nonlinear analysis by using the least number of the sophisticated higher-order element(s) with the refined plastic hinges can evaluate the behaviour of a whole reinforced concrete structure at pre-yield and post-yield stages very consistently, whose modelling capacity comprises the linear flexural cracking behaviour, gradual yielding, strain-hardening effect contributed from the reinforcement, loading redistribution due to plasticity, second-order P-δ effect, strength and stiffness deterioration due to P-Δ effect. Moreover, in order to underpin the integrated design of a RC structure using least number of element(s), several standpoints are given below,

1. Since the concrete material is non-homogenous, the evaluation of the concrete section capacity should comply with its loading distribution roughly but enough to capture the overall significant behaviour of a RC member. Hence the numerical modelling of a whole structure should be defined by the priori behavioural pattern, which can be accomplished by the automatic re-meshing process as described by Iu (2008). And the element discretisation and section properties assigned according to the priori behavioural pattern keep same in the whole loading increment of the nonlinear solution procedures.

2. A reinforced concrete member with different detailing should be divided into a number of elements complying with the corresponding reinforcement section as long as the overall significant behaviour of the RC member can be reasonably and accurately replicated, which is not sensitive but adequate.

3. The present refined plastic hinge is unfortunately only formed at the element nodes, including other conventional plastic hinge approaches, which causes the element discretisation if the material plasticity occurs along span of a member.

4. There is no ultimate error-proof element (Trifunovic and Iu (2014)) that can replicate all significant global behaviour of a member by itself. Because of this, the design of a structure with recourse to the integrated design approach is still dependent of the computer modelling, including the type of element adopted for the corresponding behaviour (i.e. its geometric and material capacity), accurate element solutions (Iu and Bradford (2015); Iu (2015)) under element loads as well as the element discretisation owing to the aforesaid causes.

Acknowledgements

References

AS3600 (2009), *Australian Standard: Concrete Structure*.

Bergan, P.G. and Holand, I. (1979), "Nonlinear finite element analysis of concrete structures", *Comput. Method. Appl. M.*, **17**, 443-467.

Branson, D.E. and Metz, G.A. (1963), "Instantaneous and time-dependent deflections of simple and continuous reinforced concrete beams", Auburn: Department of Civil Engineering and Auburn Research Foundation, Auburn University.

Bratina, S., Saje, M. and Planinc, I. (2004), "On materially and geometrically non-linear analysis of reinforced concrete planar frames", *Int. J. Solid. Struct.*, **41**(24), 7181-7207.

Chan, S.L. and Zhou, Z.H. (1994), "Pointwise equilibrating polynomial element for nonlinear analysis of frames", *J. Struct. Eng.*, **120**(6), 1703-1717.

Chen, S.F., Teng, J.G. and Chan, S.L. (2001), "Design of biaxially loaded short composite columns of arbitrary section", *J. Struct. Eng.*, **127**(6), 678-685.

Chiorean, C.G. (2010), "Computerised interaction diagrams and moment capacity contours for composite steel-concrete cross-sections", *Eng. Struct.*, **32**(11), 3734-3757.

Cope, R.J. and Rao, P.V. (1977), "Nonlinear finite element analysis of concrete slab structures", *Proceedings of Institution of Civil Engineers*, **63**, 159-179.

Cranston, W.B. (1965), "Tests on reinforced frames. I: Pinned portal frames", Technical Report, Cement and Association, London.

De Normalisation, C.E. (2004), "Design of concrete structures-Part 1-1: General rules and rules for buildings", Eurocode 2, EN 1992-1-1: 2004: E.

Espion, B. (1993), "Benchmark examples for creep and shrinkage analysis computer programs", *Creep and Shrinkage of concrete*, TC114 RILEM. E&FN Spon.

Iu, C.K. (2008), "Inelastic finite element analysis of composite beams on the basis of the plastic hinge approach", *Eng. Struct.*, **30**(10), 2912-2922.

Iu, C.K. (2015), "Generalised element load method for first-and second-order element solutions with element load effect", *Eng. Struct.*, **92**, 101-111.

Iu, C.K. and Bradford, M.A. (2012), "Higher-order non-linear analysis of steel structures. Part I: elastic second-order formulation", *Adv. Steel Constr.*, **8**(2), 168-182.

Iu, C.K. and Bradford, M.A. (2012), "Higher-order non-linear analysis of steel structures. Part II: refined plastic hinge formulation", *Adv. Steel Constr.*, **8**(2), 183-198.

Iu, C.K. and Bradford, M.A. (2015), "Novel non-linear elastic structural analysis with generalised transverse element loads using a refined finite element", *Adv. Steel Constr.*, **11**(2), 223-249.

Iu, C.K. and Chan, S.L. (2004), "A simulation-based large deflection and inelastic analysis of steel frames under fire", *J. Constr. Steel Res.*, **60**, 1495-1524.

Iu, C.K., Bradford, M.A. and Chen, W.F. (2009), "Second-order inelastic analysis of composite framed structures based on the refined plastic hinge method", *Eng. Struct.*, **31**(3), 799-813.

Izzuddin, B.A. and Lloyd Smith, D. (2000), "Efficient nonlinear analysis of elasto-plastic 3D R/C frames using adaptive techniques", *Comput. Struct.*, **78**(4), 549-573.

Izzuddin, B.A., Karayannis, C.G. and Elnashai, A.S. (1994), "Advanced nonlinear formulation for reinforced concrete beam-column", *J. Struct. Eng.*, **120**(10), 2913-2934.

Liu, S.W., Liu, Y.P. and Chan, S.L. (2012a), "Advanced analysis of hybrid steel and concrete frames. Part 1: Cross-section analysis technique and second-order analysis", *J. Constr. Steel Res.*, **70**, 326-336.

Liu, S.W., Liu, Y.P. and Chan, S.L. (2012b), "Advanced analysis of hybrid steel and concrete frames: part 2: refined plastic hinge and advanced analysis", *J. Constr. Steel Res.*, **70**, 337-349.

Ma, S.Y.A. and May, I.M. (1986), "The Newton-Raphson method used in the non-linear analysis of concrete structures", *Comput. Struct.*, **24**(2), 177-185.

Sun, C.H., Bradford, M.A. and Gilbert, R.I. (1994), "A reliable numerical method for simulating the post-failure behaviour of concrete frame structures", *Comput. Struct.*, **53**(3), 579-589.

Trifunovic, M. and Iu, C.K. (2014), "Nonlinear geometric and material computational technique: Higher-order element with refined plastic hinge approach", *International Conference on Steel, Space and Composite Structures*, Prague, Czech Republic, **12**, 387-396.

Zienkiewicz, O.C. and Taylor, R.L. (1991), *The Finite Element Method*, 4th edition, McGraw-Hill.

CC